HHS Public Access

Author manuscript

Biochemistry. Author manuscript; available in PMC 2019 May 08.

Published in final edited form as:

Biochemistry. 2018 May 08; 57(18): 2694–2703. doi:10.1021/acs.biochem.8b00262.

Dynamic Consequences of Mutation of Tryptophan 215 in Thrombin

Riley Peacock[1], **Jessie Davis**[1], **Phineus R. L. Markwick**[2], and **Elizabeth A. Komives**[1]

[1]Department of Chemistry and Biochemistry, University of California, San Diego, 9500 Gilman Drive, La Jolla, CA 92093-0378 USA

[2]San Diego Supercomputer Center University of California, San Diego 10100 Hopkins Dr, La Jolla, CA 92093 USA

Abstract

Thrombin normally cleaves fibrinogen to promote coagulation, however, binding of thrombomodulin to thrombin switches the specificity of thrombin toward protein C, triggering the anticoagulation pathway. The W215A thrombin mutant was reported to have decreased activity towards fibrinogen without significant loss of activity towards protein C. To understand how mutation of Trp215 may alter thrombin specificity, hydrogen-deuterium exchange experiments (HDXMS), accelerated molecular dynamics (AMD) simulations, and activity assays were carried out to compare the dynamics of Trp215 mutants with those of wild type (WT) thrombin. Variation in NaCl concentration had no detectable effect on the sodium-binding ($220s_{CT}$) loop, but appeared to affect other surface loops. Trp215 mutants showed significant increases in amide exchange in the $170s_{CT}$ loop consistent with a loss of H-bonding in this loop identified by the AMD simulations. The W215A thrombin showed increased amide exchange in the $220s_{CT}$ loop and in the N-terminus of the heavy chain. The AMD simulations showed that a transient conformation of the W215A thrombin has a distorted catalytic triad. HDXMS experiments revealed that mutation of Phe227, which engages in a pi-stacking interaction with Trp215, also caused significantly increased amide exchange in the $170s_{CT}$ loop. Activity assays showed only the F227V mutant had wild type catalytic activity, whereas all other mutants showed markedly lower activity. Taken together, the results explain the reduced pro-coagulant activity of the W215A mutant and demonstrate the allosteric connection between Trp215, the sodium-binding loop and the active site.

Corresponding author: Elizabeth A. Komives, Department of Chemistry and Biochemistry, University of California, San Diego, 9500 Gilman, Drive, La Jolla, CA 92092-0378, Ph: (858) 534-3058, ekomives@ucsd.edu.

Supporting Information

1. Detailed information about Accelerated Molecular Dynamics
2. Figure S1: Coverage map for HDXMS for all thrombin mutants
3. Figure S2: Deuterium uptake plots for WT and W215A thrombins 100 mM and 300 mM NaCl
4. Figure S3: Deuterium uptake plots for all other thrombin mutants at 100 mM NaCl

To accommodate readers who use one of several different numbering schemes for thrombin, we report residues in the chymotrypsin numbering which is used in PDB files of all serine proteases in which loops are denoted 60A, 60B, etc. The chymotrypsin numbering is denoted with a subscript CT, and is followed by the sequential numbering, which is more useful for describing HDXMS data, given in parentheses.

Keywords

serine protease; protein dynamics; hydrogen-deuterium exchange; allostery

Introduction

Thrombin is a dual action serine protease that binds and cleaves a variety of substrates (1). Substrate recognition is dependent on the binding of a consensus sequence at the primary specificity pockets (S1-4) within the active site, as well as binding at distinct exosites located on opposites sides of thrombin. Central to its role in the clotting cascade, thrombin distinguishes between substrates that elicit either a procoagulative or an anticoagulative response. The binding of thrombomodulin (TM) to anion binding site 1 (AEB1) of thrombin shifts the enzyme's specificity away from procoagulative substrates, such as fibrinogen and the protease-activated receptor 1(PAR1), and towards the anticoagulative substrate, protein C (PC) (2). How TM binding to thrombin alters its substrate specificity is still not fully understood. Comparison of the X-ray crystal structures of apo-thrombin and thrombin bound to TM456, a construct of TM containing only the domains necessary for toggling thrombin's substrate specify, shows no discernable differences between the two structures (3). Thus, TM-binding affects thrombin in ways that are invisible to X-ray crystallography.

Di Cera determined that the W215A mutant of thrombin had significantly less activity towards procoagulative substrates, yet this mutant retained most of the activity towards PC in the presence of TM (4). Interestingly, the W215I mutation had significantly less activity towards both procoagulative and anticoagulative substrates (5). Measurements of hirudin binding to three $Trp215_{CT}$ mutants showed that mutations at position 215_{CT} make thrombin much less sensitive to sodium binding, offering an explanation for the decreased activity observed for procoagulative substrates (4, 6). Saturation mutagenesis of $Trp215_{CT}$ revealed an array of activity profiles that distinguish $Trp215_{CT}$ mutants in their abilities to cleave fibrinopeptide A (FpA), PAR1, and PC (5), suggesting that this residue is involved in key aspects of modulating thrombin's activity. The dramatic effect of mutations at $Trp215_{CT}$ on substrate specificity identifies this residue as one of significant interest, warranting further study of how the characteristics $Trp215_{CT}$ mutants differ from those of WT thrombin.

Thrombin is a highly dynamic enzyme. Studies have demonstrated that the surface loops of thrombin exhibit dynamic motions (7, 8). Previous work from our lab has also connected the dynamic motions of thrombin to key catalytic regions of the protein, providing evidence for dynamic allostery (9, 10). Here we focus on $Trp215_{CT}$ to gain a clearer picture of how this mutation affects thrombin dynamics and activity. Due to the apparent pi-stacking interaction between $Trp215_{CT}$ and $Phe227_{CT}$ in the X-ray crystal structure of thrombin (Protein Data Base (PDB) ID code 1PPB) (11), we included mutants of $Phe227_{CT}$ in our study as well. We used a combination of activity assays, HDXMS to evaluate the differences in backbone dynamics, and AMD to obtain a molecular mechanism of changes in amide exchange.

HDXMS provides a measure of the backbone dynamics and solvent accessibility changes that occur on physiologically relevant time scales (12). HDXMS has already been used to compare the dynamics of apo-thrombin, PPACK-thrombin, and TM-thrombin, revealing

changes in surface loop dynamics that directly impact thrombin activity (13, 14). Thus, HDXMS provides a tool for comparing the backbone dynamics of thrombin mutants with the motions native to WT thrombin.

AMD is an efficient and versatile enhanced conformational space sampling algorithm that allows for the accurate study of slow motions in bio-molecular systems up to time-scales several orders of magnitude greater than those accessible using standard classical MD methods, while still affording a fully atomistic representation of the system. The acceleration level used here has previously been shown to afford an increase in the rate of conformational space sampling by 3-4 orders of magnitude (15, 16).

We show that the W215A mutant has markedly increased dynamics in the $170s_{CT}$ loop, the $220s_{CT}$ loop, and the N-terminus of the heavy chain and its dynamics are less sensitive to NaCl concentration. Investigation of the pi-stacking interaction between $Phe227_{CT}$ and $Trp215_{CT}$ revealed that this interaction is critical for ordering the $170s_{CT}$ loop, but $Trp215_{CT}$ alone is responsible for long-range allostery that impacts the $220s_{CT}$ loop and the N-terminus of the heavy chain. The results of this study clarify the previously observed coupling between sodium binding and mutation of $Trp215_{CT}$ and reveal the dramatic changes in thrombin dynamics that result from mutations at both $Trp215_{CT}$ and $Phe227_{CT}$.

Materials and Methods

Thrombin mutagenesis and Expression

All mutants were generated through site-directed mutagenesis using primers purchased from Integrated DNA Technologies. All thrombin constructs were expressed and refolded in *E. coli*, as previously described (8). Activation of thrombin was achieved by diluting properly-folded thrombin, purified through ion exchange chromatography, to 50 mL with 50 mM Tris/HCl pH 7.4, 20 mM $CaCl_2$, 1 mg/mL PEG8000, 5% (v/v) glycerol, and 20 μg/mL *E. carinatus* venom (Sigma-Aldrich Car. # V8250) pretreated with AEBSF. Optimal activation times varied from 2-10hr at room temperature, determined by monitoring the conversion of pre-thrombin-2 to a-thrombin through ion exchange chromatography. Activated samples were loaded onto a MonoS cation exchange column (GE Healthcare Life Sciences), allowing for the separation of active a-thrombin from preactive (prethombin-2, meizothrombin) and autoproteolyzed forms (particularly γ-thrombin) using a gradient of 100 mM NaCl to 500 mM NaCl in 25 mM phosphate pH 6.5. Because of their inherent inactivity, thrombin mutants F227A and W215I were activated with 45 nM wild type α-thrombin present. Fully active α-thrombin is the latest eluting species from the MonoS column, however, all fully active mutants eluted earlier than WT, allowing for effective purification of F227A and W215I from the WT thrombin added for activation. Fractions containing fully activated thrombin were pooled and stored at −80 C for no longer than 1 month before use. This method of thrombin purification, which avoids dialysis, has been shown previously to result in >95% active α-thrombin. Previous NMR analysis of isotopically labeled thrombin prepared this way, demonstrated that the species present was active a-thrombin (8, 17).

Thrombin activity assays

To account for the loss of A_{280} for all Trp mutants, enzyme concentrations were determined using BCA protein assays. Activity assay reactions occurred in 200 μL volumes containing 2.5 ng/mL human thrombin, 0.88 μM BSA, 2.93 mM $CaCl_2$, 20 mM Tris, 200 mM NaCl, and chromogenic substrate (Diapharma, West Chester, OH). Chromogenic substrate stocks at 12.5 mg/mL in H_2O were stored at −20 C, and were neutralized with Tris base before use. Chromogenic substrate dilutions were performed using a solution of 20 mM Tris and 200 mM NaCl. The thrombin-specific chromogenic substrate S-2238 was present at concentrations varying from 2.5 - 100 μM for WT, 6.25 - 200 μM for W215A, 1 - 100 μM for F227V, and 25 - 1000 μM for W215I. Activated PC (aPC)-specific chromogenic substrate S-2366 was present between 10 - 1000 μM for WT, 10 - 1000 μM for W215A, 50 - 1600 μM for F227V, and 50 - 1600 μM for W215I. All reactions were incubated at room temperature for 10 min following the addition of thrombin, before chromogenic substrate was added. Enzyme dilutions were made by diluting purified thrombin with a solution of 20 mM Tris pH 7.5, 200 mM NaCl, 5 mM $CaCl_2$, and 15 μM BSA. Each reaction was monitored via the linear increase in absorbance at 405 nm over time, corresponding to the release of p-nitroaniline following chromogenic substrate cleavage. From the rates measured, K_M and V_{max}, and thereby k_{cat}, values were determined for each substrate for each thrombin construct. All chromogenic substrate assays were repeated in triplicate.

Protein C assays were carried out as previously described (18). The TM activation of thrombin towards protein C cleavage was first performed by incubating the TM construct TM456m with purified human α-thrombin before adding protein C (Hematologic Technologies, Essex Junction, VT). TM456m was purified as previously described (14). Following a 20 min incubation with protein C, the thrombin was inactivated by addition of heparin-antithrombin-III, and the activated protein C was assayed by the addition of S-2366. Human thrombin was present at 17.4 ng/mL for each reaction, and TM456m was present at either 21.7 ng/mL, 43.5 ng/mL, 65.2 ng/mL, or 87.0 ng/mL. The rates measured in reactions from which thrombin and/or TM4546m were omitted were subtracted from the rates of the other reactions to account for any PC activation not catalyzed by the thrombin-thrombomodulin complex. The rates for each F227V reaction were divided by the rates for each WT thrombin reaction with the same amount of TM456m added, and all ratios calculated were averaged.

Fibrinogen clotting assays were performed as previously described (19). Thrombin concentrations were determined by BCA assays. The concentrations of thrombin used correspond to the amount necessary for a clot to form between 18-22 sec after the addition of fibrinogen. All clotting assays were performed in triplicate, and the average time-to-clot was used in activity determination.

Hydrogen-Deuterium Exchange Mass Spectrometry

All α-thrombin proteins were prepared for HDXMS from frozen aliquots (~7 uM). After being passed through a 0.2 micron filter, a portion was diluted to 5 μM, and 130 μL was saved for the HDXMS experiment. The remaining sample was concentrated to 10 μM using pre-rinsed 6 mL 10K MWCO Amicon concentrators, spinning at 3000 rpm in 5 min

intervals at 4°C to be used for peptide identification (50 μL). In the HDXMS experiment, the sample is diluted 12-fold (see below) resulting in a final α-thrombin concentration of 420 nM.

HDXMS was performed using a Waters Synapt G2Si system with HDX technology (Waters Corporation). Deuterium exchange reactions were prepared using a Leap HDX PAL autosampler (Leap Technologies, Carrboro, NC). D_2O buffer was prepared by lyophilizing 1 mL of 250 mM phosphate pH 6.5 and either 1 M NaCl for low salt experiments of 3 M NaCl for high salt experiments, before being resuspended in 10 ml 99.96% D_2O immediately before use. Each deuterium exchange time point (0 min, 30 sec, 1 min, 2 min, 5 min) was measured in triplicate. For each deuteration time point, 5 μL of protein was held at 25°C for 5 min before being mixed with 55 μL of D_2O buffer. The deuterium exchange was quenched for 1 min at 1°C by combining 50 μL of the deuteration reaction with 50 μL of 250 mM TCEP pH 2.5. The quenched sample was then injected in a 50 μL sample loop, followed by digestion on an in-line pepsin column (immobilized pepsin, Pierce, Inc.) at 15°C. The resulting peptides were captured on a BEH C18 Vanguard pre-column, separated by analytical chromatography (Acquity UPLC BEH C18, 1.7 uM, 1.0 × 50 mm, Waters Corporation) using a 7-85% acetonitrile in 0.1% formic acid over 7.5 min, and electrosprayed into the Waters Synapt G2Si quadrupole time-of-flight mass spectrometer. The mass spectrometer was set the collect data in the Mobility, ESI+ mode; mass acquisition range of 200-2,000 (m/z); scan time 0.4 s. Continuous lock mass correction was accomplished with infusion of leu-enkephalin (m/z = 556.277) every 30 s (mass accuracy of 1 ppm for calibration standard).

For peptide identification, the mass spectrometer was set to collect data in MS^E, mobility ESI+ mode instead. Peptides masses were identified from triplicated analyses of 10 μM α-thrombin, and data were analyzed using PLGS 2.5 (Waters Corporation). Peptides masses were identified using a minimum number of 250 ion counts for low energy peptides and 50 ion counts for their fragment ions; the peptides also had to be larger than 1500 Da. The following cutoffs were used to filter peptide sequence matches: minimum products per amino acid of 0.2, minimum score of 7, maximum MH+ error of 5 ppm, a retention time RSD of 5%, and the peptides had to be present in two of the three ID runs collected. The peptides identified in PLGS were then analyzed in DynamX 3.0 (Waters Corporation). The relative deuterium uptake for each peptide was calculated by comparing the centroids of the mass envelopes of the deuterated samples with the undeuterated controls following previously published methods (20). To account for back-exchange, and systematic autosampler sample handling differences between shorter and longer deuteration times, the uptake and standard deviation values for the 30 sec and 1 min, and the 2 min and 5 min timepoints were divided by 0.67 and 0.64 respectively for every HDXMS experiment run. Data were plotted as number of deuterons incorporated vs. time (min). The Y-axis limit for each plot reflects the total number of amides within the peptide that can possible exchange. Each plot includes the peptide MH+ value, sequence, and sequential residue numbering.

To monitor sodium binding, the HDXMS experiments were conducted at either 100 or 300 mM NaCl. Under these conditions of the HDXMS experiment (420 nM thrombin), the sodium binding site should have been less than 80% occupied at 100mM NaCl and over

90% occupied at 300 mM NaCl (21). Our previous studies have shown that for weak binding ligands, observation of “protection” of the surface of the protein requires the binding site to be over 90% occupied (22). Therefore, we expected to see the largest difference in surface “protection” by comparing 80% bound to >90% bound sodium.

AMD simulations

Atomic coordinates for WT thrombin were obtained from the Protein Data Bank (PDB) 1.9-A X-ray crystal structure (PDB ID: 1PBB) and the active-site inhibitor was removed from the structure. For the W215A mutant, residue 215_{CT} was manually converted from a tryptophan to an alanine residue. Each system was placed at the center of a periodically repeating box, and the simulation cell size was defined such that the distance between the edge of the simulation box and the surface of the solute was at least 12 Å. All AMD simulations were performed in explicit solvent with appropriate counter-ions to achieve cell neutrality. Bonds involving protons were constrained using the SHAKE algorithm. Electrostatic interactions were treated using the particle mesh Ewald method with a direct space sum limit of 10 Å. The ff14SB force-field was used for the solute residues, and the TIP3P water force-field was employed for solvent molecules. In the present work, we implemented a “dual boost” AMD approach (23), in which two acceleration potentials are simultaneously applied to the system: The first acceleration potential is applied to the torsion terms only, and a second, weaker acceleration is applied across the entire potential. For both WT thrombin and the W215A mutant systems, the specific torsional acceleration parameters were defined as Eb(dih) -<V0(dih)> = [4.0 kcal/mol * Number of residues], and the acceleration parameter, α(dih), was set to one-fifth of this value. The total background acceleration parameters were fixed at Eb(tot) -<V0(tot)> = α(tot) = [0.16 kcal/mol * No. atoms in simulation cell]. The specific choice of these AMD parameters was based on a previous NMR/AMD study of thrombin:PPACK (8). The results of this and other studies suggested that these acceleration parameters afforded an effective speed up in conformational space sampling of 3-4 orders of magnitude, which is in line with other studies on different systems in which AMD simulations at a similar acceleration level were directly compared to long brute-force CMD simulations (16). More details about how the acceleration is achieved in AMD are given in the Supplementary Information. The average minimum energy potentials, V0(dih) and V0(tot), were obtained from 20-ns CMD simulations performed as part of the initial equilibration procedure. It should be noted that, given the similarity of the two systems, the acceleration parameters for WT thrombin and the W215A mutant are, to all intents and purposes, identical.

For each system (WT and W215A thrombin), two AMD simulations were performed for 750,000,000 steps with a (real time) time-step of 2-fs. This is computationally equivalent to performing a 1.5μs CMD simulation. Given an effective speed up in the rate of conformational space-sampling by 3 to 4 orders of magnitude due to the application of the bias potential, we anticipate that the configurational space sampling afforded in each of the AMD simulations is associated with slow time-scale dynamics occurring on time-scales of milliseconds to tens of milliseconds, thereby identifying slow motions, including rare local unfolding/refolding events which can be experimentally probed by HDXMS in the fast limit. All simulations were performed using the AMBER14 simulation suite. For each AMD

trajectory, a corrected canonical ensemble was obtained by performing the Boltzmann free energy reweighting protocol using a cumulant expansion to the second order (24).

Results

Improved HDXMS of thrombin

In order to determine the effects of sodium concentration and the W215A mutation on thrombin dynamics, HDXMS experiments were carried-out. WT and each mutant thrombin were allowed to exchange into deuterated buffer for 0-5 min followed by quenching in 100 mM tris-carboxyethylphosphine, pH 2.5, which improved sequence coverage after pepsin digestion. Fifty-one peptides were reliably identified, which covered 99.0% of the thrombin sequence. Due to the location of the mutations examined, the peptides covering the $220s_{CT}$ loop varied depending on the mutation (Figure S1). To probe the dependence of the thrombin dynamics on NaCl concentration, experiments on WT and W215A thrombin were carried out at 100 mM NaCl and 300 mM NaCl.

The effect of W215A and Salt on the $220s_{CT}$ Loop

We first analyzed the difference in deuterium uptake of W215A and WT thrombin in 100 mM vs. 300 mM NaCl. As previously reported by DiCera's group, the W215A mutation renders thrombin much less sensitive to Na^+ ions (4). The deuterium uptake within the W215A $220s_{CT}$ loop (residues 260-275; MH+ 1673.760, 1788.801) appeared unaffected by NaCl concentration, resulting in similar uptake values at both NaCl concentrations (Figure 1). Interestingly, the $220s_{CT}$ loop in WT thrombin also showed nearly identical deuterium uptake at 100 mM and 300 mM NaCl. The $220s_{CT}$ loop of the W215A mutant showed notably higher deuterium uptake compared to WT thrombin, by an average of ~2 deuterons at both the high and low salt concentrations. These results indicate that the $220s_{CT}$ loop is sensitive to dynamic modulation caused by changes to side chains at the base of the loop, but its dynamics appear insensitive to NaCl concentration.

Subtle effects caused by NaCl

Several other functionally interesting regions of thrombin did show a moderate dependence of deuterium uptake on NaCl concentration. The deuterium uptake in regions located near anion binding sites 1 (AEB1) and 2 (AEB2) were affected by the concentration of salt more so than by the W215A mutation. Residues $66\text{-}85_{CT}$ (residues 97-117; MH+ 2586.441) showed a slight increase in deuterium uptake with decreasing salt concentration but residues $66\text{-}80_{CT}$ (residues 97-112; MH+ 2014.105) showed no difference, allowing us to localize the salt effect to residues $81\text{-}85_{CT}$ (residues 113-117) (Figure 2). This trend extended through residues $85\text{-}102_{CT}$ (residues 117-135; MH+ 2530.295), which approaches AEB2 and includes $Asp102_{CT}$ of the catalytic triad. Similarly, residues $117\text{-}129_{CT}$ (residues 150-162; MH+ 1513.747) showed no dependence on NaCl concentration, but residues $117\text{-}130_{CT}$ (residues 150-166; MH+ 1897.984) were affected by salt indicating residues $129A\text{-}130_{CT}$ (residues 163-166) of ABE2 also respond to salt concentration. Slight salt effects were observed for other surface loops including the $180s_{CT}$ loop (residues 223-255; MH + 3575.589), the $140s_{CT}$ loop (residues 181-196; MH+ 1714.912), the $30s_{CT}$ loop (residues

55-64; MH+ 1220.646), and the light chain (residues 1-15; MH+ 1569.737 and residues 16-31; MH+ 1934.008) (Figure S2).

The effect of the W215A mutation and NaCl on the 170s$_{CT}$ loop

Unlike the 220s$_{CT}$ loop, both NaCl and the W215A mutation significantly affected deuterium uptake. Three peptides -residues 156-180$_{CT}$ (residues 197-221; MH+ 2896.550), 161-170$_{CT}$ (residues 202-211; MH+ 1155.619), and residues 161-181$_{CT}$ (residues 202-222; MH+ 2490.296) covered the 170s$_{CT}$ loop and portions of the C-terminal β-barrel (Figure 3). The combination of the W215A mutation and low NaCl concentration resulted in the highest exchange, and this region of the W215A mutant thrombin incorporated an average of ~4 more deuterons over 5 min as compared to WT thrombin.

The effect of W215A and NaCl on the N-Terminus of the heavy chain

The N-terminus of the heavy chain, residues 16-23$_{CT}$ (residues 37-44; MH+ 819.373) exhibited a slight increase in uptake at lower NaCl as well as in the presence of the W215A mutation (Figure 4A). Thus, the dynamics of the N-terminus of the heavy chain are also affected by NaCl and the W215A mutation.

Accelerated MD simulations of the W215A mutant thrombin

In order to complement the experimental HDXMS data, we performed extensive accelerated molecular dynamics (AMD) simulations (25, 26) on both WT thrombin and the W215A mutant (see Methods for details). AMD simulations were performed for 750,000,000 steps using a “real time” time step of 2fs, the equivalent of 1.5μs in a classical MD simulation. Because the acceleration level used here affords an increase in the rate of conformational space sampling by 3-4 orders of magnitude, the simulations presented here probe slow molecular motions occurring on timescales of milliseconds to tens of milliseconds (16).

In agreement with the experimental HDXMS data, comparative analysis of the conformational dynamics from AMD simulations of WT and W215A thrombin revealed, for the most part, very few differences between WT and the W215A mutant. The most significant difference observed was a transient destabilization of the 170s$_{CT}$ loop (residues 205-223) in the W215A mutant on slow timescales. Mutation of Trp215$_{CT}$ to Ala removes the strong ring-ring stacking interaction between Trp215$_{CT}$ (residue 263) and Phe227$_{CT}$ (residue 275), causing enhanced mobility on slow timescales of residue Phe227$_{CT}$ and its neighbor, Tyr228$_{CT}$ (residue 276). As a result, transient dislocation of H-bond interactions between residues Tyr228$_{CT}$ and Phe181$_{CT}$ (Tyr276:NH-Phe222:CO and Phe222:NH-Tyr276:CO) is observed. The loss of these H-bonds apparently results in transient unfolding of the alpha-helix residues Arg165-Ser171$_{CT}$ (residues 206-212) with further dislocation of the H-bonds between residues Val167$_{CT}$, Glu164$_{CT}$, Lys169$_{CT}$, Arg165$_{CT}$, and Ser171$_{CT}$(residues Val208:NH-Glu205:CO, Lys210:NH-Arg206:CO, and Ser212:NH-Val208:CO). It should be noted that the local unfolding events described above are rare, and approximate free energy statistics obtained from the AMD simulations suggest that the population of this locally unfolded structural motif is less than 10%. These results are consistent with the experimental HDXMS results which showed an increased uptake of four additional deuterons in residues 156-181$_{CT}$ (197-222) for the W215A mutant thrombin (cf.

Figure 3). The AMD simulation results suggest that the four amide protons are those of residues Arg 165_{CT}, Val167_{CT}, Lys169_{CT}, and Ser171_{CT} (residues Arg206, Val208, Lys210, and Ser212).

In addition to the transient destabilization of the $170s_{CT}$ loop, the AMD simulations also identified a different transient conformation of the W215A mutant which was characterized by a dramatic shift in the side chains of Phe227_{CT} and Ile16_{CT} (residue 37) resulting in a misalignment of the catalytic triad (Figure 4B). A full description of the AMD simulations, including a computational analysis of the HDXMS data will be presented elsewhere (P.R.L Markwick, R. Peacock, E.A. Komives, manuscript submitted).

Determination of the role of Trp215 in stabilizing the thrombin structure

Because Trp215_{CT} appears to be undergoing pi-stacking with Phe 227_{CT} (11), we wondered whether the F227A mutation would have the same effects as the W215A mutation. In addition, the more conservative substitutions W215I and F227V were also prepared and all of the mutants were subjected to HDXMS under conditions where the enzyme appears to be most dynamic (100 mM NaCl). The W215A, W215I, and F227A mutants all showed similarly increased deuterium uptake in residues 156-180_{CT} (residues 197-221; MH + 2896.550) and residues 161-181_{CT} (residues 202-222 MH+ 2490.296) as compared to WT thrombin (Figure 5A). Comparison of the deuterium uptake in the overlapping peptide, residues 161-170_{CT} (202-211; MH+ 1155.619), suggested the increased deuterium uptake was at least partially occurring in the α-helix spanning residues 165-170_{CT} (residues 206-211) in all mutants, however the W215I mutation did not destabilize to the same extent. All of the mutants also showed increased deuterium uptake in the $220s_{CT}$ loop -residues 208-227_{CT} (residues 256-275; MH+ 2152.943, MH+ 2191.954, and MH+ 2267.985 for W215A, F227A, and WT respectively), residues 212-227_{CT} (residues 260-275; MH + 1673.760, MH+ 1715.806, and MH+ 1788.801 for W215A, W215I, and WT respectively), and residues 212-228_{CT} (residues 260-276; MH+ 1903.864 for F227V) -relative to wild type thrombin (Figure 5B), although the increase in uptake for F227V could not be accurately determined as there was no matching peptide in the WT dataset.

Evidence for exposure of the Trp215 backbone amide

Although increased deuterium uptake in peptides spanning the $220s_{CT}$ loop was observed for the Trp215_{CT} and Phe227_{CT} mutants, examination of the deuterium uptake into two overlapping peptides spanning residues 208-215_{CT} (residues 256-263) in WT, F227A and F227V allowed assignment of a significant portion of the effect to the backbone amide at position 215_{CT} (residue 263). By subtracting the deuterium uptake into the peptide spanning residues 208-214_{CT} (residues 256-262; MH+ 797.386) from that of the peptide spanning residues 208-215_{CT} (residues 256-263; MH+ 983.466), it was possible to determine that a full additional amide was exchanged into position 215_{CT} in the F227A mutant and a stepwise increase in deuterium uptake with decreasing hydrophobic character in the sidechain of residue 227_{CT} (Figure 5C). Thus, the hydrophobicity of the residue at position 227 affects the exchange of the amide group at position 215.

Understanding the HDXMS results in light of thrombin catalytic activity

Because HDXMS showed that mutation of W215A, W215I, F227A, and F227V affected the dynamics of the loops surrounding the thrombin active site, the catalytic activity of these mutants was characterized using chromogenic substrates that target only the active site. The catalytic ability of W215A, W215I, and F227A towards the coagulative substrates fibrinopeptide A (FPA) and protease-activated receptor 1 (PAR1), and the anticoagulative substrate protein C (PC) have already been characterized (5). When expressing and purifying the various mutants as fusion constructs containing 18 residues from prothrombin, we noticed that W215A and F227V were able to catalyze the self-cleavage of the propeptide which occurs after cleavage of the activation peptide by ecarin. W215I and F227A required the addition of WT thrombin to affect the self-cleavage. Consistent with its ability to self-cleave, the F227V mutant retained significant activity towards all substrates tested compared to WT thrombin (Table 1). Although W215A could self-cleave, its activity was decreased to less than 10% of WT thrombin in chromogenic substrate assays as well as towards fibrinogen. The mutants W215I and F227A, lost their ability to self-activate, and were not studied further due to their lack of observed activity.

We compared two chromogenic substrates, the S-2238, which has a bulky Phe at P3 and is thought to mimic fibrinogen, vs. S-2366, which has a smaller pyroGlu at P3 and is thought to mimic protein C and PAR1. Though WT thrombin was able to cleave both chromogenic substrates, each mutant preferentially cleaved the procoagulant mimicking substrate S-2238, which is best exemplified by F227V (Table 1).

Discussion

The effect of NaCl on the dynamics of thrombin

Even though the sodium binding site was identified between the $220s_{CT}$ and $180s_{CT}$ loops (21, 27), our HDXMS results did not show a difference in dynamics in these loops at NaCl concentrations between 100 mM NaCl and 300 mM NaCl for WT thrombin. These concentrations were chosen to maximize the difference in surface “protection” by a ligand with a millimolar binding constant (22). Other regions did show differences in exchange at 100 vs 300 mM NaCl indicating that differences could be observed under the experimental conditions. The region of thrombin that showed the most significant sensitivity to NaCl concentration was the $170s_{CT}$ loop (residues 197-222; $156\text{-}181_{CT}$), which did not show an appreciable difference in conformation between the sodium-free and sodium bound forms according to crystallographic evidence (28). Mutation of $Trp215_{CT}$ did cause a significant increase in the dynamics of the $220s_{CT}$ loop indicating that its motions can, in fact, be altered. Di Cera has previously reported that mutation of Trp 215_{CT} appears to decrease the Na-binding affinity of thrombin as indicated by hirudin binding (4). Our results suggest that $Trp215_{CT}$ is coupled to the $220s_{CT}$ loop but that Na affects the conformational states of the 170s loop and the N-terminus of the heavy chain which would also be expected to alter activity and hirudin binding.

Other effects of NaCl concentration observed were almost entirely localized to the surface loops of thrombin, in both WT thrombin and the W215A mutant. Interaction of monovalent

ions interact with regions of thrombin distinct from the $220s_{CT}$ and $180s_{CT}$ loops was proposed previously based on MD simulations (29) and Xiao et al. showed that the surface loops of thrombin displayed a smaller ensemble of conformations upon interaction with sodium ions (30). In fact, we show decreased amide exchange in the surface loops at higher NaCl concentrations consistent with these simulation results. Our results also showed a marked sodium-induced stabilization of the $90s_{CT}$ loop (residues 117-135), which contains $Asp102_{CT}$, and this may actually be the major underlying cause of observed effects of sodium ions on thrombin activity.

The effect of mutations at Trp215 and Phe227 on local structure

Just as a lower concentration of NaCl leads to increased deuterium uptake in the $170s_{CT}$ loop and the β-strands that flank it, so does the interruption of the pi-stacking interaction between the side chain at positions 215_{CT} and 227_{CT}. When the side chain at either position was replaced with Val or Ile, the $170s_{CT}$ loop was slightly more stabilized than for the alanine mutants. Analysis of the deuterium uptake into residues $156\text{-}181_{CT}$ (residues 197-222) in conjunction with the hydrogen bonds broken during the AMD simulations of W215A localized the amides that are likely undergoing increased amide exchange in the $Trp215_{CT}$ and $Phe227_{CT}$ mutants to those within the $170s_{CT}$ loop itself.

Uniqueness of the $Trp215_{CT}$-$Phe227_{CT}$ interaction

$Trp215_{CT}$ is nearly perfectly conserved across the chymotrypsin family of serine proteases, although $Phe227_{CT}$ is not. Val or Ile is found at position 227_{CT} for all members in the coagulation protease family except for thrombin. It was recently shown that the $170s_{CT}$ loop in murine urokinase-type plasminogen activator (muPA), which contains a Val at position 227_{CT}, exists in equilibrium between two distinct, highly dynamic conformations that require the $Cys168_{CT}$-$Cys182_{CT}$ bond to “adopt different rotational conformers to allow” for interconversion (31). This result is consistent with our observation that the F227V mutant has higher exchange in the $170s_{CT}$ loop. Conventional molecular dynamics simulations analyzed using a Markov state model showed that trypsin, which also has a Val at position 227_{CT}, samples conformational states where the side chain of $Trp215_{CT}$ is rotated towards the active site (32). In fact, there are many apparently stabilizing interactions that $Trp215_{CT}$ makes with residues in the $170s_{CT}$ loop including interaction with $Ile174_{CT}$. Additional interactions within the $170s_{CT}$ loop that don’t directly involve $Trp215_{CT}$ include the interaction between $Thr172_{CT}$ and $Glu217_{CT}$. Given that the T172A, I174A, E217A, and F227A all exhibit the same ~10-fold decrease in activity towards FpA and PAR1, while retaining protein C activation (5), we may speculate that these side chains all work together to optimize thrombin’s procoagulative function.

The residue at position 215_{CT} may flip into the active site

Multiple other studies have shown that the $Trp215_{CT}$ side chain of thrombin can occlude the active site upon mutation of residues near the active site such as D102N (33), Δ146-149e (34), Y225P (35), and N143P (36). In MD simulations, WT thrombin adopts a similar occluded conformational state in a sodium-free environment (30). When analyzing the effects of W215A, W215I, and F227V on the activity of thrombin towards substrates, we observed that the activity of W215I towards both chromogenic substrates was strikingly

diminished compared to the W215A mutant. The F227A mutant also could not self-activate and this could be due to a reconfiguration of the $Trp215_{CT}$ side chain into the active site preventing optimal activity. In contrast, the F227V mutant is able to self-activate, cleave fibrinogen, and activate PC with near WT activity. A consistent model that explains these data is that a Val at position 227_{CT}, as is found in all other coagulation proteases, is sufficient to stabilize the $Trp215_{CT}$ side chain from flipping into the active site whereas an Ala at position 227_{CT} is not. Additionally, the $Ile215_{CT}$ interaction with $Phe227_{CT}$ is not as optimal as the interaction of $Trp215_{CT}$ with $Val227_{CT}$ resulting in the repositioning of $Ile215_{CT}$ into the active site blocking activity. These data show the importance of introducing multiple conservative substitutions for understanding the role of specific enzyme residues as well as the importance of correlating data from HDXMS with enzyme activity.

The HDXMS data presented here show that the backbone amide of $Trp215_{CT}$ in WT thrombin does exchange with deuterated solvent, but at a rate far slower than nearly all other regions of the enzyme. The presence of $Phe227_{CT}$ in thrombin may be an evolutionarily significant event allowing the S1 site to more often be open for substrate binding. Consequently, the catalytic triad of thrombin would be stabilized to a greater degree than is observed for other chymotrypsin-like proteases.

Long-range effects of mutation of Trp215

Mutations at $Trp215_{CT}$ appeared to have a greater effect on deuterium exchange into the $220s_{CT}$ loop than mutations at 227_{CT} suggesting that the W215A mutation destabilized residues in the $220s_{CT}$ loop to a greater extent than the F227A mutation. Although mutations at $Phe227_{CT}$ led to the increased exchange into the backbone amide of $Trp215_{CT}$, only mutations at $Trp215_{CT}$ appeared to notably affect amide exchange into the whole $220s_{CT}$ loop.

Our HDXMS results also showed that the W215A mutant had significantly higher exchange into the N-terminus of the heavy chain, and this effect was greater than for any of the other mutants tested (Figure 4A and S3). The AMD simulations of the W215A mutant showed a transient structure in which the side chain of $Phe227_{CT}$ (residue 275) was rotated into the position that the $Trp215_{CT}$ side chain formerly occupied. Huntington and Esmon also observed a shift in the position of $Phe227_{CT}$ in the crystal structure of the S195A mutant (37). In our AMD simulations of the W215A mutant, the side chain of $Arg173_{CT}$ (residue 214) also rotated to form a new interaction with $Glu217_{CT}$ (residue 265). Interestingly, the structure of the W215A/E217A double mutant thrombin (38, 39) showed the $214\text{-}219_{CT}$ segment collapsed into the S1 pocket similar to the structures of D102N (33), Δ146-149e (34), Y225P (35), and N143P (36). Our AMD results suggest that removal of the $Trp215_{CT}$ side chain transforms the backbone of residues $214\text{-}219_{CT}$ into a much less structured segment, stabilized only when the side chain of $Arg173_{CT}$ makes contact with $Glu217_{CT}$. Kinetic analysis of R173A by Di Cera et al. showed no significant deviation of activity towards either procoagulative or anticoagulative substrates as compared to WT thrombin (5), but it is possible that the Arg173-$Glu217_{CT}$ interaction stabilizes the $214\text{-}219_{CT}$ segment only when $Trp215_{CT}$ is also mutated. This would explain why the double W215A/E217A mutant shows a collapsed S1 pocket in X-ray crystal structures (38). Our results thus provide

the first experimental evidence of the allosteric connections between position 215_{CT} and the active site first proposed by Di Cera (33, 38).

The AMD results show that the structural effects of the altered $214\text{-}219_{CT}$ segment are accompanied by a shift in the backbone hydrogen bonding to the N-terminal amino group of $Ile16_{CT}$ (residue 37) and a reorientation of the $Ile16_{CT}$ side chain. In addition, the side chains of $Asp194_{CT}$ (residue 240) and $Ser195_{CT}$ (residue 241) are altered resulting in improper alignment of the serine hydroxyl group with $His57_{CT}$ (residue 79) (Figure 4B). Finally, $Asp189_{CT}$ (residue 235) at the base of the S1 pocket is also rotated almost 180° away from its position in the wild type enzyme and forms a new H-bond with $Arg187_{CT}$ (residue233) which is now located in the sodium binding pocket.

The work presented here identifies the distinct changes in the structure of thrombin that result from both changes in the concentration of NaCl and the disruption of the $Trp215_{CT}$-$Phe227_{CT}$ pi-stacking interaction. Our results explain how the $170s_{CT}$ loop, which makes up part of ABE2, may act as another potential regulatory region of thrombin. Additionally, the similar effects of NaCl concentration and the disruption of the $Trp215_{CT}$-$Phe227_{CT}$ pi interaction on the $170s_{CT}$ loop of thrombin opens the door for questions regarding whether sodium ions help modulate this pi interaction. Most importantly, the combination of HDXMS, which provides evidence of structural changes that are difficult to elucidate by crystallographic methods alone, with AMD simulations, provides a clearer understanding of allostery in thrombin. Here we show that mutation of $Trp215_{CT}$ rebalances the ensemble of states to populate structures in which the $170s_{CT}$ loop is unfolded and structures in which the catalytic triad and S1 pocket are perturbed. Future experiments that investigate the dynamics of thrombin will be imperative for developing a full picture regarding complex enzyme regulation.

Supplementary Material

Refer to Web version on PubMed Central for supplementary material.

Acknowledgments

This work was supported by NIH grant HL070999. RP acknowledges support from the Molecular Biophysics Training Grant T32 GM008326.

References

1. Bode W. The structure of thrombin: a janus-headed proteinase. Semin Thromb Hemost. 2006; 32:16–31. [PubMed: 16673263]
2. Esmon CT. Regulation of blood coagulation. Biochim Biophys Acta. 2000; 1477:349–360. [PubMed: 10708869]
3. Fuentes-Prior P, Iwanaga Y, Huber R, Pagila R, Rumennik G, Seto M, Morser J, Light DR, Bode W. Structural basis for the anticoagulant activity of the thrombin-thrombomodulin complex. Nature. 2000; 404:518–525. [PubMed: 10761923]
4. Arosio D, Ayala YM, Di Cera E. Mutation of W215 compromises thrombin cleavage of fibrinogen, but not of PAR-1 or protein C. Biochemistry. 2000; 39:8095–8101. [PubMed: 10891092]
5. Marino F, Pelc LA, Vogt A, Gandhi PS, Di Cera E. Engineering thrombin for selective specificity toward protein C and PAR1. J Biol Chem. 2010; 285:19145–19152. [PubMed: 20404340]

6. Ayala Y, Di Cera E. Molecular recognition by thrombin. Role of the slow– >fast transition, site-specific ion binding energetics and thermodynamic mapping of structural components. J Mol Biol. 1994; 235:733–746. [PubMed: 8289292]
7. Lechtenberg BC, Johnson DJ, Freund SM, Huntington JA. NMR resonance assignments of thrombin reveal the conformational and dynamic effects of ligation. Proc Natl Acad Sci U S A. 2010; 107:14087–14092. [PubMed: 20660315]
8. Fuglestad B, Gasper PM, Tonelli M, McCammon JA, Markwick PR, Komives EA. The dynamic structure of thrombin in solution. Biophys J. 2012; 103:79–88. [PubMed: 22828334]
9. Gasper PM, Fuglestad B, Komives EA, Markwick PR, McCammon JA. Allosteric networks in thrombin distinguish procoagulant vs. anticoagulant activities. Proc Nat Acad Sci. 2012; 109:21216–21222. [PubMed: 23197839]
10. Handley LD, Fuglestad B, Stearns K, Tonelli M, Fenwick RB, Markwick PR, Komives EA. NMR reveals a dynamic allosteric pathway in thrombin. Sci Rep. 2017; 7:39575. [PubMed: 28059082]
11. Bode W, Mayr I, Baumann U, Huber R, Stone SR, Hofsteenge J. The refined 1.9 A crystal structure of human alpha-thrombin: interaction with D-Phe-Pro-Arg chloromethylketone and significance of the Tyr-Pro-Pro-Trp insertion segment. The EMBO Journal. 1989; 8:3467. [PubMed: 2583108]
12. Truhlar SM, Croy CH, Torpey JW, Koeppe JR, Komives EA. Solvent accessibility of protein surfaces by amide H/2H exchange MALDI-TOF mass spectrometry. J Am Soc Mass Spectrom. 2006; 17:1490–1497. [PubMed: 16934999]
13. Koeppe JR, Seitova A, Mather T, Komives EA. Thrombomodulin tightens the thrombin active site loops to promote protein C activation. Biochemistry. 2005; 44:14784–14791. [PubMed: 16274226]
14. Handley LD, Treuheit NA, Venkatesh VJ, Komives EA. Thrombomodulin binding selects the catalytically active form of thrombin. Biochemistry. 2015; 54:6650–6658. [PubMed: 26468766]
15. Cervantes CF, Markwick PR, Sue SC, McCammon JA, Dyson HJ, Komives EA. Functional dynamics of the folded ankyrin repeats of I kappa B alpha revealed by nuclear magnetic resonance. Biochemistry. 2009; 48:8023–8031. [PubMed: 19591507]
16. Kamenik AS, Kahler U, Fuchs JE, Liedl KR. Localization of millisecond dynamics: Dihedral entropy from accelerated MD. J Chem Theory Comput. 2016; 12:3449–3455. [PubMed: 27322931]
17. Baerga-Ortiz A, Rezaie AR, Komives EA. Electrostatic dependence of the thrombin-thrombomodulin interaction. J Mol Biol. 2000; 296:651–658. [PubMed: 10669614]
18. White CE, Hunter MJ, Meininger DP, White LR, Komives EA. Large-scale expression, purification and characterization of small fragments of thrombomodulin: the roles of the sixth domain and of methionine 388. Protein Engineering, Design and Selection. 1995; 8:1177–1187.
19. Fenton JW. Thrombin. Annals New York Acad Sci. 1986; 485:5–15.
20. Wales TE, Fadgen KE, Gerhardt GC, Engen JR. High-speed and high-resolution UPLC separation at zero degrees Celsius. Anal Chem. 2008; 80:6815–6820. [PubMed: 18672890]
21. Di Cera E, Guinto ER, Vindigni A, Dang QD, Ayala YM, Wuyi M, Tulinsky A. The Na+ binding site of thrombin. J Biol Chem. 1995; 270:22089–22092. [PubMed: 7673182]
22. Mandell JG, Baerga-Ortiz A, Akashi S, Takio K, Komives EA. Solvent accessibility of the thrombin-thrombomodulin interface. J Mol Biol. 2001; 306:575–589. [PubMed: 11178915]
23. Hamelberg D, de Oliveira CA, McCammon JA. Sampling of slow diffusive conformational transitions with accelerated molecular dynamics. J Chem Phys. 2007; 127:155102. [PubMed: 17949218]
24. Miao Y, Sinko W, Pierce L, Bucher D, Walker RC, McCammon JA. Improved Reweighting of Accelerated Molecular Dynamics Simulations for Free Energy Calculation. J Chem Theory Comput. 2014; 10:2677–2689. [PubMed: 25061441]
25. Hamelberg D, Mongan J, McCammon JA. Accelerated molecular dynamics: a promising and efficient simulation method for biomolecules. J Chem Phys. 2004; 120:11919–11929. [PubMed: 15268227]
26. Markwick PR, McCammon JA. Studying functional dynamics in bio-molecules using accelerated molecular dynamics. Phys Chem Chem Phys. 2011; 13:20053–20065. [PubMed: 22015376]

27. Zhang E, Tulinsky A. The molecular environment of the Na+ binding site of thrombin. Biophys Chem. 1997; 63:185–200. [PubMed: 9108691]
28. Pineda AO, Carrell CJ, Bush LA, Prasad S, Caccia S, Chen ZW, Mathews FS, Di Cera E. Molecular dissection of Na+ binding to thrombin. J Biol Chem. 2004; 279:31842–31853. [PubMed: 15152000]
29. Kurisaki I, Takayanagi M, Nagaoka M. Toward Understanding Allosteric Activation of Thrombin: A Conjecture for Important Roles of Unbound Na+ Molecules around Thrombin. J Phys Chem B. 2015; 119:3635–3642. [PubMed: 25654267]
30. Xiao J, Melvin RL, Salsbury FR. Mechanistic insights into thrombin's switch between "slow" and "fast" forms. Phys Chem Chem Phys. 2017; 19:24522–24533. [PubMed: 28849814]
31. Kromann-Hansen T, Lange EL, Sørensen HP, Hassanzadeh-Ghassabeh G, Huang M, Jensen JK, Muyldermans S, Declerck PJ, Komives EA, Andreasen PA. Discovery of a novel conformational equilibrium in urokinase-type plasminogen activator. Sci Rep. 2017; 7:3385. [PubMed: 28611361]
32. Plattner N, Noé F. Protein conformational plasticity and complex ligand-binding kinetics explored by atomistic simulations and Markov models. Nat commun. 2015; 6
33. Gandhi PS, Chen Z, Mathews FS, Di Cera E. Structural identification of the pathway of long-range communication in an allosteric enzyme. Proc Nat Acad Sci. 2008; 105:1832–1837. [PubMed: 18250335]
34. Bah A, Carrell CJ, Chen Z, Gandhi PS, Di Cera E. Stabilization of the E* form turns thrombin into an anticoagulant. J Biol Chem. 2009; 284:20034–20040. [PubMed: 19473969]
35. Niu W, Chen Z, Gandhi PS, Vogt AD, Pozzi N, Pelc LA, Zapata F, Di Cera E. Crystallographic and kinetic evidence of allostery in a trypsin-like protease. Biochemistry. 2011; 50:6301–6307. [PubMed: 21707111]
36. Niu W, Chen Z, Bush-Pelc LA, Bah A, Gandhi PS, Di Cera E. Mutant N143P reveals how Na+ activates thrombin. J Biol Chem. 2009; 284:36175–36185. [PubMed: 19846563]
37. Huntington JA, Esmon CT. The molecular basis of thrombin allostery revealed by a 1.8 A structure of the "slow" form. Structure. 2003; 11:469–479. [PubMed: 12679024]
38. Pineda AO, Chen ZW, Caccia S, Cantwell AM, Savvides SN, Waksman G, Mathews FS, Di Cera E. The anticoagulant thrombin mutant W215A/E217A has a collapsed primary specificity pocket. J Biol Chem. 2004; 279:39824–39828. [PubMed: 15252033]
39. Gandhi PS, Page MJ, Chen Z, Bush-Pelc L, Di Cera E. Mechanism of the anticoagulant activity of thrombin mutant W215A/E217A. J Biol Chem. 2009; 284:24098–24105. [PubMed: 19586901]

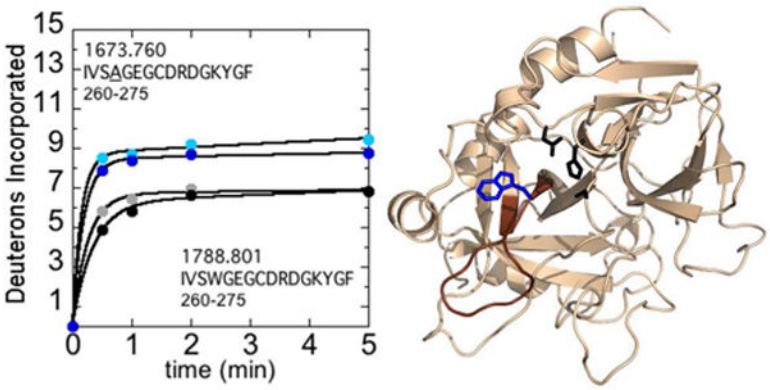

Figure 1.

A) Deuterium incorporation into residues 212-227$_{CT}$ (residues 260-275; MH+ 1673.760 and 1788.801 for W215A and WT respectively) over 5 min is shown for WT thrombin at 100 mM NaCl (grey) and 300 mM NaCl (black), and for the W215A mutant at 100 mM NaCl (cyan) and 300 mM NaCl (blue). The mutant residue, is underlined in the peptide sequence shown. B) Structure of WT thrombin (PDB 1PPB) highlighting residues 212-227$_{CT}$ (residues 260-275; brown). The sidechains of Trp215$_{CT}$ (blue) and the catalytic triad (black) are shown as sticks.

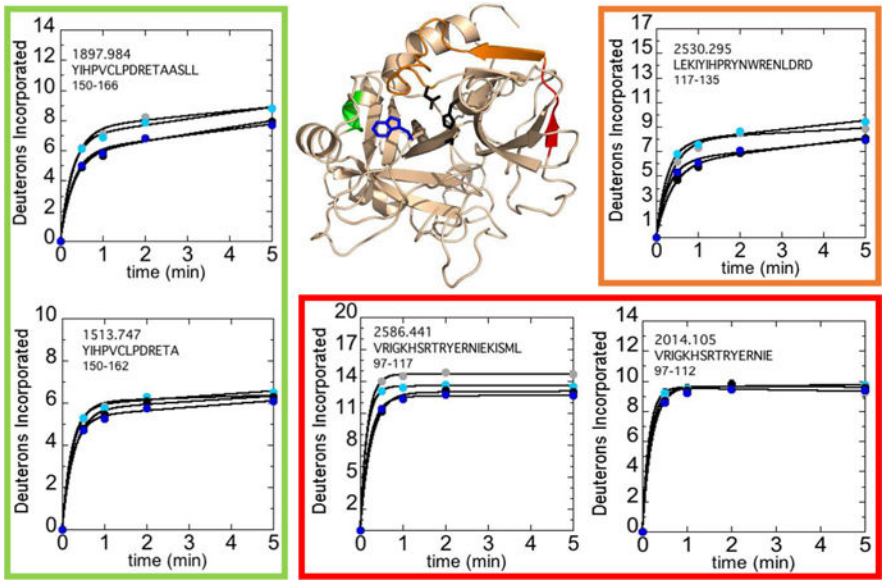

Figure 2.

Structure of WT thrombin (PDB 1PPB) highlighting residues 81-85$_{CT}$ (residues 113-117; red), residues 86-102$_{CT}$ (residues 118-135; orange), and residues 129A-130$_{CT}$ (residues 163-166; green). Colored residues specify regions affected by the concentration of NaCl after subtraction of deuteron uptake of overlapping peptides 66-80$_{CT}$ (residues 97-112; MH + 2014.105) from 66-85$_{CT}$ (residues 97-117; MH+ 2586.441) and 117-129$_{CT}$ (residues 150-162; MH+ 1513.747) from 117-130$_{CT}$ (residues 150-166; MH+ 1897.984) as well as residues 85-102$_{CT}$ (residues 117-135; MH+ 2530.295). The sidechains of Trp215$_{CT}$ (blue) and the catalytic triad (black) are shown as sticks. Deuteron incorporation into these residues over 5 min is shown for WT thrombin at 100 mM NaCl (grey) and 300 mM NaCl (black), and for the W215A mutant at 100 mM NaCl (cyan) and 300 mM NaCl (blue).

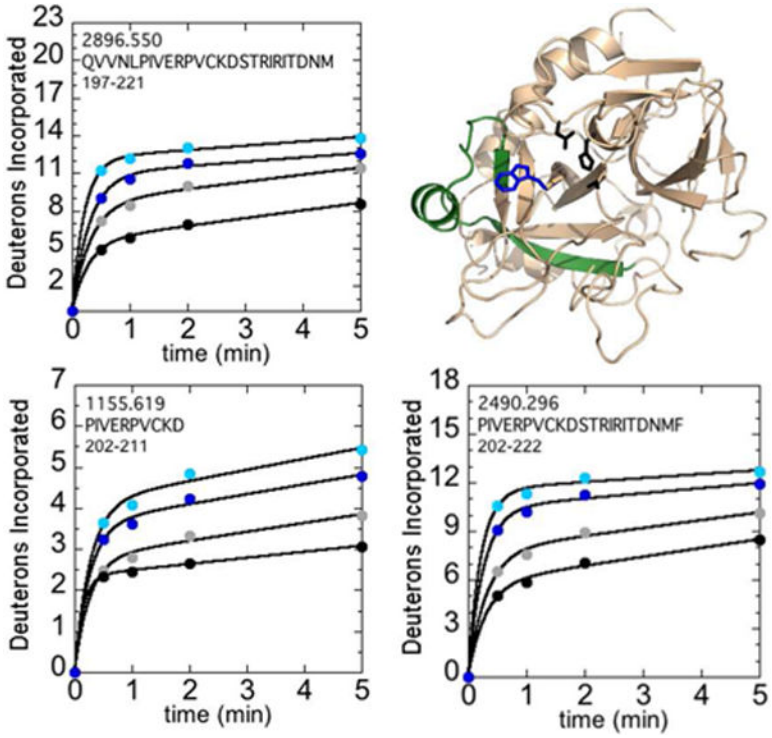

Figure 3.

Structure of WT thrombin (PDB 1PPB) highlighting 156-181$_{CT}$ (residues 197-222; green). The sidechains of Trp215CT (blue) and the catalytic triad (black) are shown as sticks. Deuteron incorporation over 5 min into residues 156-180$_{CT}$ (residues 197-221; MH + 2896.550), 161-170$_{CT}$ (residues 202-211; MH+ 1155.619), and 161-181$_{CT}$ (residues 202-222; MH+ 2490.296) is shown for WT thrombin at 100 mM NaCl (grey) and 300 mM NaCl (black), and for the W215A mutant at 100 mM NaCl (cyan) and 300 mM NaCl (blue).

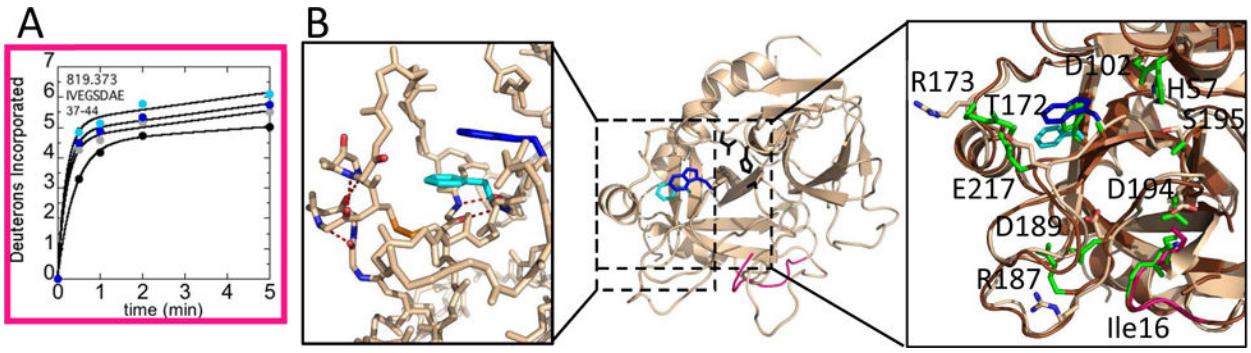

Figure 4.

A) Deuterium incorporation over 5 min into residues 16-23$_{CT}$ (residues 36-44; MH + 819.373) for WT thrombin at 100 mM NaCl (grey) and 300 mM NaCl (black), and for the W215A mutant at 100 mM NaCl (cyan) and 300 mM NaCl (blue). **B)** Structure of WT thrombin (wheat; PDB 1PPB) highlighting residues 16-23$_{CT}$ (pink). The sidechains of Trp215$_{CT}$ (blue), Phe227$_{CT}$ (cyan), and the catalytic triad (black) are shown as sticks. Accelerated MD simulations identified 5 H-bonds (red-dotted lines) within WT thrombin (left) that broke during simulations of W215A. The transient structure observed during the W215A simulation (brown) overlaying the structure of WT thrombin (right). The side chains of His57$_{CT}$, Asp102$_{CT}$, Thr172$_{CT}$, Arg173$_{CT}$, Arg 187$_{CT}$, Asp 189$_{CT}$, Asp194$_{CT}$, Ser195$_{CT}$, Trp215$_{CT}$ (blue), Glu217$_{CT}$, and Phe227$_{CT}$ (cyan). The 140s$_{CT}$ loop is hidden for clarity. The backbone of Ile16$_{CT}$ (pink) is also shown as sticks. The corresponding side chains in the W215A structure, including Ala215$_{CT}$, are colored green and are shown as sticks.

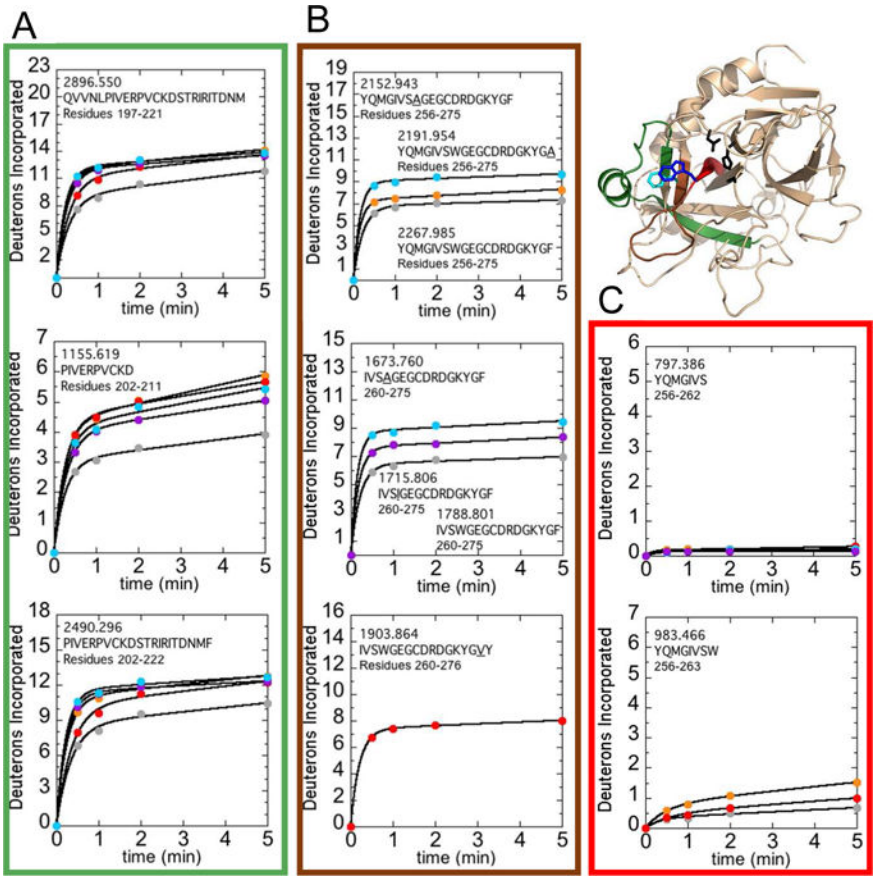

Figure 5.

Structure of WT thrombin (PDB 1PPB) highlighting residues 156-181$_{CT}$ (residues 197-222; green), residues 208-215$_{CT}$ (residues 256-263; red), and residues 216-228$_{CT}$ (residues 264-276; brown). The sidechains of Trp215$_{CT}$ (blue), Phe227$_{CT}$ (cyan), and the catalytic triad (black) are shown as sticks. **A)** Uptake plots corresponding to residues 156-180$_{CT}$ (residues 197-221; MH+ 2896.550), 161-170$_{CT}$ (residues 202-211; MH+ 1155.619), and 161-181$_{CT}$ (residues 202-222; MH+ 2490.296). **B)** Uptake plots corresponding to residues 208-227$_{CT}$ (residues 256-275; MH+ 2152.943, MH+ 2191.954, and MH+ 2267.985 for W215A, F227A, and WT respectively), residues 212-227$_{CT}$ (residues 260-275; MH + 1673.760, MH+ 1715.806, and MH+ 1788.801 for W215A, W215I, and WT respectively), and residues 212-228$_{CT}$ (residues 260-276; MH+ 1903.864 for F227V). The mutant residue, if present, is underlined in the peptide sequence shown. **C)** Uptake plots corresponding to residues 208-214$_{CT}$ (residues 256-262; MH+ 797.386) and 208-215$_{CT}$ (residues 256-263; MH+ 983.466). Deuterium incorporation over 5 min into the multiple peptides that cover these regions are shown for WT thrombin (grey) as well as the F227A (orange), F227V (red), W215A (cyan), and W215I (purple) mutants under experimental conditions of 100 mM NaCl.

Table 1

Activity of the various thrombin mutants.

Construct	S elf-Activating?	s/s_{WT} S-2238	s/s_{WT} S-2366	Fibrinogen Activation units relative to WT thrombin	Protein C activation rate relative to WT thrombin
WT	Yes	1.00+/−0.16	1.00+/−0.03	1	1
W215A	Yes	0.053+/− 0.007	0.038+/− 0.003	0.034+/−0.002	n.d.
W215I	No	0.017+/− 0.001	0.013+/− 0.003	n.d.	n.d.
F227A	No	n.d.	n.d.	n.d.	n.d.
F227V	Yes	1.00+/−0.15	0.66+/−0.06	0.86+/−0.06	0.66+/−0.07

s/s_{WT} is the ratio of k_{cat}/K_M for the mutant divided by the k_{cat}/K_M for the wild type. Fibrinogen activation units correspond to the amount of thrombin required to clot fibrinogen in 20 sec. This amount for WT thrombin is 100 ng or 3 pmol. Protein C activation was determined as described in the Methods section.